Hydrogeol J (2017) 25:557–574
DOI 10.1007/s10040-016-1491-y

REPORT

River–groundwater connectivity in a karst system, Wellington, New South Wales, Australia

Mohammadreza Keshavarzi[1] · **Andy Baker**[1] · **Bryce F. J. Kelly**[1] · **Martin S. Andersen**[1,2]

Received: 22 April 2016 / Accepted: 28 October 2016 / Published online: 7 December 2016

Abstract The characterization of river–aquifer connectivity in karst environments is difficult due to the presence of conduits and caves. This work demonstrates how geophysical imaging combined with hydrogeological data can improve the conceptualization of surface-water and groundwater interactions in karst terrains. The objective of this study is to understand the association between the Bell River and karst-alluvial aquifer at Wellington, Australia. River and groundwater levels were continuously monitored, and electrical resistivity imaging and water quality surveys conducted. Two-dimensional resistivity imaging mapped the transition between the alluvium and karst. This is important for highlighting the proximity of the saturated alluvial sediments to the water-filled caves and conduits. In the unsaturated zone the resistivity imaging differentiated between air- and sediment-filled karst features, and in the saturated zone it mapped the location of possible water- and sediment-filled caves. Groundwater levels are dynamic and respond quickly to changes in the river stage, implying that there is a strong hydraulic connection, and that the river is losing and recharging the adjacent aquifer. Groundwater extractions (1,370 ML, megalitres, annually) from the alluvial aquifer can cause the groundwater level to fall by as much as 1.5 m in a year. However, when the Bell River flows after significant rainfall in the upper catchment, river-leakage rapidly recharges the alluvial and karst aquifers. This work demonstrates that in complex hydrogeological settings, the combined use of geophysical imaging, hydrograph analysis and geochemical measurements provide insights on the local karst hydrology and groundwater processes, which will enable better water-resource and karst management.

Keywords Karst · Groundwater/surface-water relations · Electrical resistivity imaging · Groundwater management · Australia

Introduction

Enhanced knowledge of surface-water and groundwater interactions is required to inform water resources policy and management, and environmental studies. When and how water transfers between a river and an underlying aquifer remains poorly understood in many areas throughout the world (Ivkovic 2009). This is especially true in karst basins, where delineation of surface-water and groundwater connectivity is more difficult due to the complex fractures and solution channels in carbonates (Bailly-Comte et al. 2009; Winter 1995). The interaction between rivers and groundwater generally takes place in three basic ways (Winter et al. 1998): (1) in gaining conditions, rivers receive water from inflow of groundwater through the riverbed; (2) in losing conditions, rivers discharge surface water into groundwater by outflow through the riverbed; or (3) gaining in some reaches of the river and losing in other reaches, or both lose and gain in the same reach at different times. For example, Andersen and Acworth (2009) analyzed the annual flow difference between two gauge stations on the Namoi River in north-eastern New South Wales, Australia, and they revealed that losses from the river are remarkably larger than the combined surface-water diversion and groundwater extraction.

✉ Mohammadreza Keshavarzi
m.keshavarzi@unsw.edu.au

[1] Connected Waters Initiative Research Centre, UNSW Australia, Sydney, Australia

[2] School of Civil and Environmental Engineering, UNSW Australia, Sydney, Australia

In karst terrains, river water can easily infiltrate the adjacent aquifer due to features such as fractures and solution cavities (Brown et al. 2014; Gulley et al. 2011). In particular, underground karst features have strong anisotropy, which dominates subsurface flow directions (Palmer 1986); however, karst aquifers have complex and distinct characteristics, often with high flow in only a small portion of the rock mass, which makes them very different from other aquifers (Bakalowicz 2005; Bonacci et al. 2006). To manage karst systems, it is crucial to understand the interaction of groundwater and surface water (Bonacci et al. 2006), including connections to adjacent aquifer systems. Loss of surface water to karst aquifers can contribute to carbonate dissolution and increase the vulnerability of the aquifer to contamination (Brown et al. 2014; Lindsey et al. 2009; Musgrove et al. 2014).

The distribution of different lithologies, the presence of faults, fracture zones and the extent of karst rock are all potential major controls on groundwater flow in catchments that contain karst. Within karst aquifers, conduits are the most important feature that provide low resistance pathways for groundwater flow (Bonacci et al. 2006). These physical features, however, are generally complex and difficult to detect. Locating underground karstic features from the surface is one of the most challenging tasks in karst research.

The establishment of a surface-water and groundwater level monitoring network, combined with a series of non-invasive two-dimensional (2D) resistivity imaging profiles has the potential to map connectivity between a river and the underlying aquifer systems, and provide an improved geological conceptual model of the local hydrogeology. Geophysical mapping with 2D resistivity imaging is commonly applied to map subsurface lithology, to locate the transition between saturated and unsaturated zones and to delineate karst features, such as cavities (Cook and Van Nostrand 1954; Kaufmann and Romanov 2009; Leucci and De Giorgi 2005; Soupios et al. 2007; Šumanovac and Weisser 2001). Air, clay or water-filled caves, should have significant electrical resistivity contrast with the host rocks, to make them suitable targets for mapping with 2D resistivity imaging.

Wellington Caves provides a unique setting to validate the combined use of 2D resistivity imaging, hydrograph analysis, and geochemical investigations. This is because there is direct access to the karstic groundwater system, and the site has both boreholes and caves that intercept groundwater (Keshavarzi et al. 2014). These can be used to ground-truth the resistivity surveys where they intersect. In addition, Wellington Caves can be considered representative of typical limestone in Eastern Australia (Osborne 2010). These caves also hold sediments and stalagmites that are sources of information of past climates and environments (Blyth et al. 2014; Dawson 1985). The karst groundwater resource is important to the aquatic ecosystem of the Wellington Caves (Spate et al. 2001; Thurgatel et al. 2001). Prior to this research, the hydraulic connection between the Bell River and karst system was poorly understood, and subsurface cavities had not been mapped using any geophysical techniques. Understanding the local recharge mechanism and discharge from a river to the alluvium and karst is very important for the protection of the karst ecosystem and the recreational value of these caves for tourism. It is also important for providing a scientific basis for sound management of surface-water and groundwater resources of this area. Locally, a balance must be maintained between protecting groundwater movement through the karst system and supplying groundwater for irrigated agriculture immediately north of Wellington Caves.

This study demonstrates the benefits of linking hydrogeological data with 2D resistivity imaging to better understand flow paths from the river, through the alluvium and into the complex karst system at Wellington Caves, NSW, Australia. This is achieved by continuously measuring surface-water and groundwater levels, making repeated measurements of chloride concentrations in water from the river, alluvium and karst. This complex system constitutes a small-scale experimental site to study karst/river interactions that can be widely applied to other karst environments.

Methods

Site description

Geological setting

Wellington Caves Reserve is located 7 km south of the town of Wellington, central New South Wales, Australia (longitude 148° 56′ 20″ E, latitude 32° 37′ 17″ S) (Fig. 1). The Wellington Caves area is within the Garra Formation, which is Early Devonian in age (Chatterton et al. 1979; Johnson 1975; Mawson et al. 1988; Strusz 1965). Underlying the Garra Limestone are the Cuga Burga Volcanics. The Garra Formation is comprised of shallow-water limestone, with minor cherty and volcaniclastic sandstone, fissile shale and marly siltstone. In the Wellington area, limestone is the main outcrop of the Garra Formation (Johnson 1975; Strusz 1965), consisting of a thick sequence (915–1,200 m) of fossiliferous, typically thinly well-bedded and massive units. Tectonic activity by the Late Devonian (350 Ma) caused deformation and folding of Garra Formation. At Wellington Caves the limestone units, particularly the thinly bedded unit, are significantly refolded, faulted and fractured (an example is Anticline Cave, Fig. 2). Geological units are deposited in a north–south alignment. The Bell River is about 700 m to the west of Wellington Caves. Situated between the caves and the river is the river alluvium, which overlies the Garra limestone, and consists of fluvial channel sands and gravels, interbedded with overbank silt and clay deposits. The valley-filling sediments fill a paleochannel that ranges from a few meters on the margins to 35 m (based on borehole logs to the north of the caves).

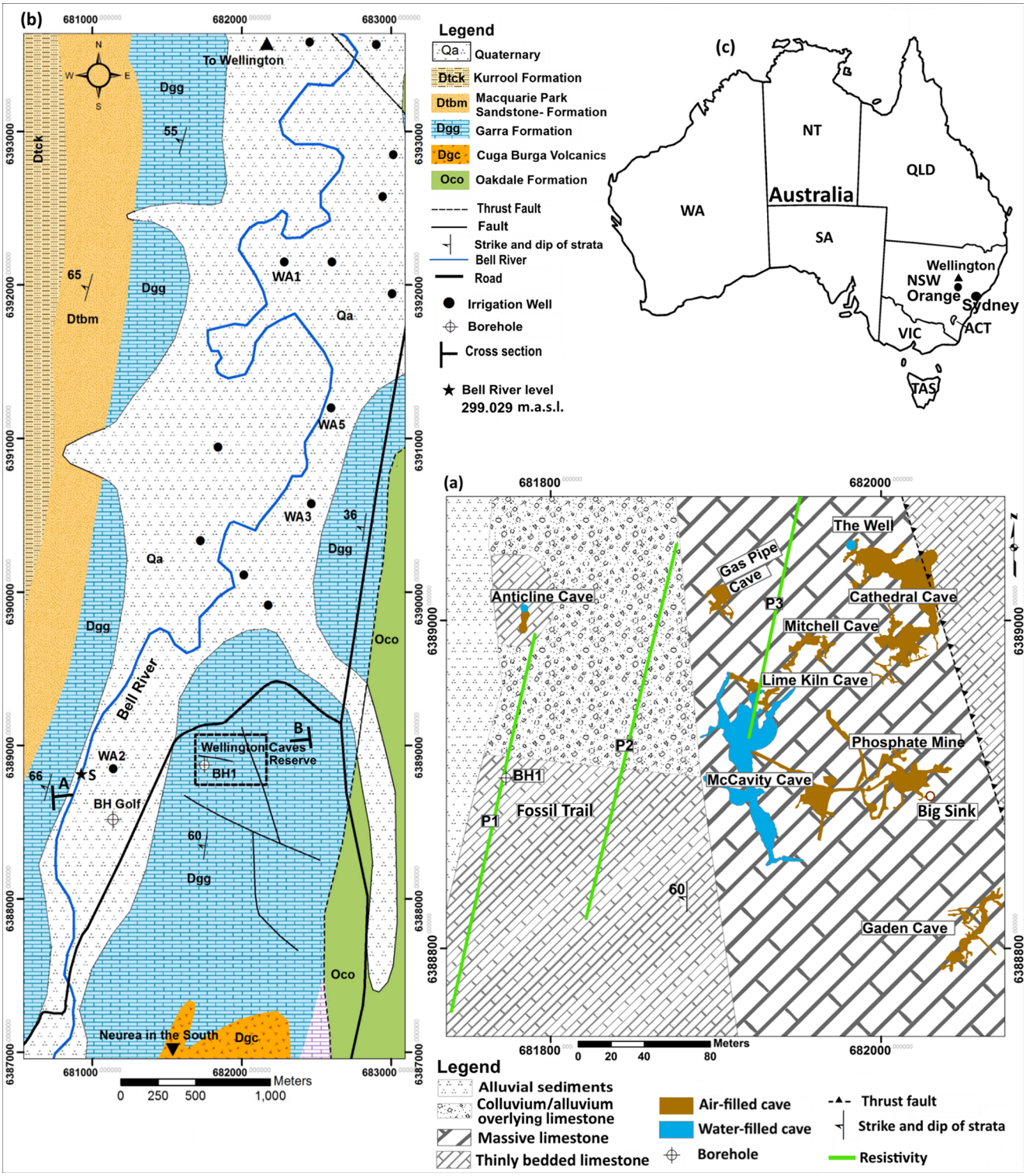

Fig. 1 **a** Wellington Caves Reserve, **b** Geological map of the study area, located 7 km south of Wellington, **c** Central Western New South Wales (NSW), Australia. Office of Water Gauge 421018) is located 5 km upstream of the study area at Neurea (to the south of the figure). Several points on the Bell River and boreholes were surveyed by DGPS (Trimble R4 GNSS System, measurements with 10–20 mm precision). Water level data at each of the boreholes (*BH Golf*, *BH1*, *Anticline* and *The Well*) and the surface-water gauge are corrected to AHD (Australian Height Datum)

The alluvial aquifer is recognized as an unconfined aquifer without any distinct layering or aquitard units. The proximity of the river, permeable alluvial sediments, and karst known for its caves suggests that there is a high potential for connectivity

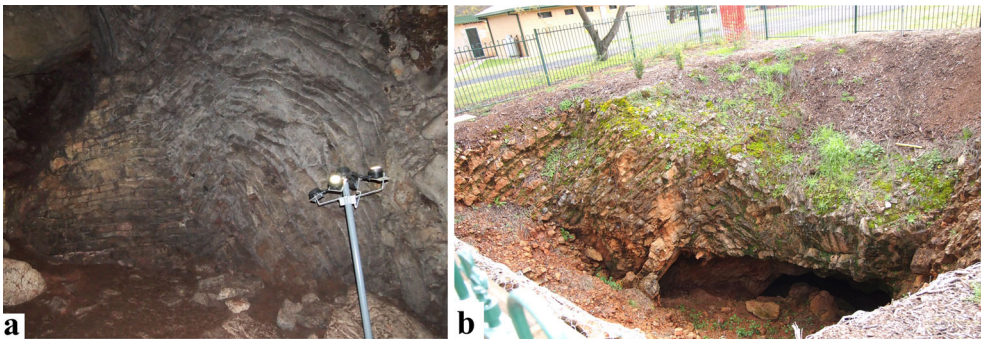

Fig. 2 Folding and fracturing of the thinly bedded limestone: **a** Anticline structure in Cathedral Cave, and **b** at entrance of Anticline Cave

between the river and the karst aquifer (Keshavarzi et al. 2014); however, hydrogeological evidence supported by geochemical analyses has yet to be applied to this region to validate the extent of connectivity.

Hydrological setting

The Bell River is a tributary of the Macquarie River, which is part of the Murray-Darling River Basin. Its 1,248 km^2 catchment area is located in central New South Wales. The river rises in the hills north-west of Orange and flows generally in a south to north direction and discharges into the Macquarie River to the north of the town of Wellington. The elevation of the study area varies from 420 to 277 m.a.s.l. (meters above sea level) and the Bell River varies from 312 to 277 m.a.s.l. The climate is temperate, semi-arid with average rainfall and potential evaporation of about 617 and 1,798.9 mm/a, respectively. The mean annual daily minimum and maximum temperatures are 9.4 and 24.4 °C, respectively. Rainfall is generally higher in the summer with the highest average monthly rainfall occurring between November and February.

The Bell River has small dams in the headwaters upstream of the study site near Orange, and substantial upstream water abstraction occurs for agriculture. The river also flows over limestone upstream of the study site. The Bell River gauge height (stage) along the study reach varies over 4 m between high-flow (floods) and low-flow conditions. There are ~20 abstraction wells for irrigation in the alluvial aquifer immediately north of the Wellington Caves Reserve. Approximately 95 %—1,370 megalitres (ML) annually—of the groundwater abstraction from the alluvium is allocated for irrigation, and 5 % (76 ML annually) is used for other rural purposes such as stock and domestic water supply. Along the alluvial floodplains immediately north of the caves, the groundwater is primarily used to produce commercial vegetable crops, grow lucerne, maize and chickpeas, and produce fodder (NSW DPI 2012).

Wellington Caves Reserve

Surface karst forms are not well developed at the Wellington Caves Reserve site. The caves are not related to the modern day topography and are therefore presumed to predate the Late Quaternary. There is evidence of hypogene cave formation in some caves (Osborne 2007), suggesting that they have been formed by both downward water movement and upward dissolution by groundwater. The seven known caves are therefore just those where the surface landscape has weathered to expose these caves. It is anticipated that there are other undiscovered caves in the area.

The seven large known caves, which are open to the surface, have mainly developed in the massive limestone units in the Garra Formation. Cathedral Cave (about 140 m in length and with a max width of 30 m) has been developed as a tourist cave, as it is the largest and most spacious cave. The main chamber of the cave intersects the boundary between the massive and thinly bedded limestone (Osborne 2001, 2007). The deepest part of Cathedral Cave, called The Well, intercepts the water table. Gas Pipe Cave (about 26 m in length and max width of 11 m) is a former tourist cave, consisting essentially of a small single room with some inactive speleothem (Osborne 2007). Mitchell Cave (about 60 m in length and max width of 10 m), 30 m west of Cathedral Cave, has a main chamber with dimensions 10 × 10 m. This cave is open to the surface through one natural and two artificial shafts. The Phosphate Mine (consisting of approximately 300 m of conduit pathways, with a maximum width of 16 m), was a partially sediment-filled cave before being mined between 1912 and 1918. Big Sink (6 × 6 m) is an old collapsed doline connected to the southwest of the Phosphate Mine. Lime Kiln Cave, to the south of Mitchell Cave and west of the Phosphate Mine cave system, is the dry part of the large McCavity Cave system (about 138 m in length and with a maximum width of 20 m). McCavity Cave is completely groundwater-filled. This cave has been extensively explored by divers since the 1980s. Gaden Cave (about 65 m in length and with a maximum width of 8 m) is a rift-like cave with no natural entrance. It is also used as a tourist cave and is located 100 m south of the Phosphate Mine. Anticline Cave (about 15 m in length and with a maximum width of 6 m), 130 m west of McCavity, is a cave developed in the thinly bedded limestone. Anticline cave also intercepts the water table.

Two-dimensional resistivity imaging

Two-dimensional (2D) resistivity imaging (also called electrical resistivity imaging, 2D resistivity profiling or more generally DC resistivity) is one of the most frequently used geophysical techniques (Loke et al. 2013). Resistivity imaging is now a mature method as a result of both technological and processing advances over the last three decades (Loke et al. 2013). With modern systems, several hundred meters of profiling can be collected in a day. The size of features that can be mapped depends on the electrode spacing, depth of the object and the contrasts in resistivity between the object of interest and the surroundings (Binley and Kemna 2005; Kaufmann and Deceuster 2014; Qarqori et al. 2012; Loke and Barker 1995; Pánek et al. 2010; Zhou et al. 2002).

Reynolds (1997), Loke (1999), and Dahlin and Zhou (2004) summarize the advantages and disadvantages of the commonly used electrode arrays (Wenner, Schlumberger and dipole-dipole) for 2D resistivity imaging. The Wenner array has the strongest signal strength compared to noise (Loke 1999), and it was for this reason that this array was selected. The Wenner array is relatively more sensitive for delineating horizontal structures, and poorer for mapping vertical structures (Loke 1999). There are also recent good examples (Nouioua et al. 2013; Redhaounia et al. 2016) that show the ability of the Wenner array to map the complex geometry of karstic subsurface conditions. Zhou et al. (2002) in their study found that the Wenner array was relatively poor at detecting sinkholes. However, in this study, an important aim was to map the transition between the unsaturated and saturated zones (which is a horizontal structure). Also, the location the major caves are well known. This help with constraining the interpretation where the resistivity profiles pass over these known caves.

Resistivity acquisition and processing

This research used 2D resistivity imaging to non-invasively investigate the location of subsurface karst features (caves) and groundwater. Electrical resistivity measurements were taken using a Terrameter SAS 4000 with the Multimac System (ABEM, Sweden) (Dahlin 2001). In June 2014, three 2D resistivity-imaging sections parallel to each other were produced. For each 2D resistivity-imaging section, a 64 electrodes array was used and 461 measurements of apparent resistivity recorded. An electrode spacing of 2.5 m was used to obtain detailed information in the shallow subsurface. The maximum effective depth of investigation for the array was 21 m. Electrode to ground contact was improved by adding salty water to the soil in the immediate zone around each electrode.

Before data processing, the resistivity data were checked for the presence of bad data points, which are discernible as anomalously high values relative to surrounding data or as isolated negative values. Large resistivity contrasts in the vicinity of the electrodes (Wilkinson et al. 2008), and strong anisotropy in subsurface resistivity (Kim et al. 2006; Nicollin et al. 2010) could give negative resistivity values. Negative values and abrupt resistivity transitions were removed before the apparent resistivity data were inverted. The robust inversion technique (Dahlin and Zhou 2004; Loke et al. 2003) was used to derive an estimate of the "true resistivity" of the subsurface. The robust inversion algorithm was selected to process the resistivity data because of the noise apparent in the near surface data, the presence of sharp boundaries between the cavities and host limestone, and to enhance the boundary between the unsaturated and saturated zones. The robust inversion method minimizes the absolute difference between the measured and apparent resistivity values, and for all inversions, the cut-off value was set to 0.005, with an RMS goal of 5 % or less.

To constrain the interpretation of the resistivity sections, resistivity measurements were referenced against outcrops of weathered and non-weathered limestone, known cavities, zones of known sediment type, the borehole lithological log, and water salinity measurements from the borehole, and karst groundwater. Values for each rock, sediment type and water at the site are listed in Table 1.

Using available subsurface data such as borehole data in conjunction with surface geophysics is essential for constraining the interpretation of the resistivity images (Acworth and Dasey 2003). The locations of 2D resistivity-imaging lines (Fig. 1a) were therefore chosen based on knowledge of the local karst geomorphology (known caves like Anticline and Lime Kiln caves). Additionally, one line was chosen to tie in with an existing borehole (BH1) in the limestone, in which the water table could be measured, and to extend across the known transition between the limestone and the alluvial sediments. It was assumed that there are some conduits and fractures where groundwater flows occur between the alluvial aquifer and the karst system; thus, the resistivity lines were also aligned to traverse across relatively flat sections to avoid topographical corrections in the inversion. Line P1 is located over the thinly bedded limestone (southern end of the line) and the alluvial sediments, which cover the karst rock (northern end of the line). Line P2 is located over the thinly bedded limestone (southern portion of the line) and the transition zone between the thinly bedded limestone, the alluvial/colluvial sediments, and the edge of the massive limestone. Line P3 traverses the massive limestone and intersects known sinkholes- and caves both air and sediment filled.

Water level analysis

Analysis of time-series records of river and groundwater levels is one of the most common methods for quantifying

Table 1 Inferred and measured resistivity values for rocks, sediments and water in the study area

Materials	Inverted resistivity (Ωm)	Measured/ inferred	Site and resistivity section reference point
Limestone	500–2,500	Measured	Limestone outcrop southern portion (right side) of sections P1 (Fig. 3) and P2 (Fig. 4).
Weathered limestone	100–500	Measured	Weathered limestone outcrops observable in sections P1, P2 and P3 (Figs. 3, 4, and 5)
Unsaturated coarse-grained sediments	100–300	Measured	Surficial dried sediments in the northern portion of resistivity section P2 (Fig. 4)
Unsaturated clayey sediments	10–50	Measured	Aeolian clayey soils and observable sinkhole filling sediments in section P3 (Fig. 5)
Saturated sediments	5–50	Inferred	Alluvial sediments below the water table in section P1 (Fig. 3)
Air-filled cavities[a]	>2,500	Inferred	Known cavities on the northern side of section P3 (Fig. 5)
Water-filled caves	5–15	Inferred	Collective insights from groundwater samples, anomaly geometry and position with respect to karst outcrop in line P1 (Fig. 3)
Groundwater sample	11	Inferred	The average EC measured at BH1 between the 24th June and 24th July was 910 μS/cm which is equal to a resistivity of 11 Ωm

[a] For air-filled cavities the resistivity value is based on the inverted resistivity from the ERT profiles

water transfer (Smakhtin 2001). Reliable groundwater level measurements are fundamental to all hydrogeological investigations (Bonacci 2015). The water level in caves (Cathedral and Anticline), the piezometric level within both the karst aquifer (BH1) and the alluvial system, and the discharge in the river upstream of the karst study region were measured to improve knowledge of river/karst interaction within the study region. The assessment of the connection between the Bell River and the adjacent alluvium and karst systems (Fig. 1) was based on data collected from a river gauge (NSW Office of Water Gauge 421018) at Neurea located upstream of the study area, three karst groundwater monitoring sites (The Well in Cathedral Cave, Anticline Cave and BH1) and the boreholes in the alluvium (BH Golf, WA2, WA3 and WA5). Groundwater level data for The Well, Anticline Cave, BH1 and BH Golf were recorded at 15-min intervals using Solinst loggers over the period 2010–2014. These data were supplemented by monitoring water levels at three irrigation bores (WA2, WA3 and WA5) in 2013–2014. The groundwater monitoring borehole elevations and the Bell River monitoring site were surveyed by DGPS (Trimble R4 GNSS System, measurements with 10–20 mm precision). Water levels data at each of the boreholes and the surface-water gauge were corrected to AHD (Australian Height Datum).

Chloride concentration

Chloride occurs naturally and is often the most dominant anion in groundwater. It is highly mobile and not involved in common geochemical reactions that occur in most aqueous environments (Freeze and Cherry 1979; Hem 1985). Kaufman and Orlob (1956) performed tracer experiments in groundwater, and found that chloride movement through most of the soils tested undergoes little or no retardation compared to other tracers. Chloride is an effective groundwater tracer because of its neutral chemical behavior (Allison and Hughes 1978; Cox et al. 2007; Harvey et al. 1989).

The groundwater sites and the Bell River were sampled monthly between January and July 2014 for chloride analysis. This work hypothesizes that, if there is a hydraulic connection as well as losing conditions in the river, any noticeable change in the surface-water chloride concentration should affect the chloride concentration in the adjacent aquifer after some lag time.

Results and interpretation

Geophysical surveys

Resistivity ranges of materials at Wellington Caves

Table 1 shows the inverted resistivity of earth materials in the study area. Air is an insulator, and theoretically, air-filled caves have a near infinite electrical resistivity compared to the host rock (here limestone); however, there are several factors which can affect the detection and the apparent resistivity of air-filled cavities as measured by ERT. These factors include the following: their volume, their depth, the physical properties of the material surroundings the caves, electrode

noise, and the type of resistivity array (Dey and Morrison 1979; Habberjam 1969; Greenfield et al. 1976; Spiegel et al. 1980; Ward 1990). In the ERT resistivity profiles and Table 1, anomalies with inverted resistivities of >2,500 Ωm were interpreted as potentially air-filled cavities. Currents pass around the cavity, and this masks their presence, but cavities are still discernible.

In the resistivity images presented, circular anomalies with an inverted resistivity greater than 2,500 Ωm are potentially air-filled caves or competent limestone. The electrical conductivity (EC) of groundwater was measured in Anticline Cave, BH1, and The Well and at the time of the resistivity surveys had an average value of 900 μS/cm, which is equal to a resistivity of 11 Ωm. The inverted resistivity values around 11 Ωm, associated with a geometry consistent with a conduit or cave, can be inferred to be water-field cavities. The weathering of limestone can cause mineralogical and geochemical transformations that may results in significant changes in the properties of the weathered limestone compared to the parent limestone (Dubois et al. 2014). Kaufmann et al. (2012) demonstrated that electrical resistivity imaging can discriminate between competent and weathered limestone when they have significantly different resistivity values. All limestone within the region is jointed and these joints, as well as some karst conduits, are commonly filled with red earth sediments from the land surface. These red earth sediments contain electrically conductive kaolinite and smectite clays (Anderson et al. 1999). In situ weathering of the limestone may also result in the formation of electrically conductive alterite, kaolinite and chlorite (Carroll and Hathaway 1953; Dubois et al. 2014). It is reasonable to expect that both the red earth sediments and the weathering products (i.e. clays and oxides) within the joints would lower the resistivity of the bulk rock mass. Competent zones of limestone ranged from 500 to 2,500 Ωm, while zones of weathered limestone had inverted resistivity values ranging from 100 to 500 Ωm. The alluvial sediments and soils had resistivity values that ranged from 10 to 300 Ωm, but decreasing with increasing degree of saturation and increasing clay content.

2D resistivity images at Wellington Caves

The resistivity surveys ranged from 157.5 to 235 m in length and provide a nearly continuous 2D image of the subsurface cross-sections (Figs. 3a, 4a, and 5a). The root-mean-squared error (RMS) between the calculated and measured apparent resistivity values was between 1.8 and 4.7 %. All three resistivity sections show multiple resistivity anomalies.

Profile line P1 (Fig. 3) was surveyed over the shallow karst aquifer within the thinly bedded limestone (see Fig. 1a for location). The borehole BH1 (Fig. 3c) along this 2D resistivity-imaging line is a control point, and is located in the thinly bedded limestone. It intercepts a small narrow cavity, which contains groundwater at a depth of 11 m. This inverted resistivity cross-section has an RMS error of 1.8 %, which indicates that the model is a feasible solution. There is a steeply dipping boundary between the low resistivity alluvial sediments in the north (left side of Fig. 3a) and the relatively more electrically resistive thinly bedded limestone in the south (right side of Fig. 3a). The surface projection of the boundary starts at 90 m and dips towards the north. From the borehole at 92 m, it is known that there is a small conduit at this location. However, this feature is not observable in the resistivity section, which highlights that resistivity imaging using the Wenner array can only delineate large-scale karst features in the order of meters.

It appears from the section that the borehole is in a more weathered portion of the thinly bedded limestone (inverted resistivity values 100–500 Ωm). To the south, there are portions of the sections with readings greater than 500 Ωm, consistent with a more compacted rock. There is an anomaly with inverted resistivity values less than 15 Ωm at 60 m along the profile and a depth of 10–21 m below the ground surface. This may be a water-filled cave in the karst aquifer system, which could be a pathway for groundwater flow between the alluvial and karst aquifers. Alternatively, it could be a clay-rich zone. At this location, the water table is 10.7 m below the ground surface. The water levels in both borehole BH1 and Anticline Cave, 10 m south of this profile, are similar, indicating a possible hydraulic connection through a conduit or a fracture zone.

Portions of outcropping limestone were observed from BH1 to 200 m along the resistivity profile (Fig. 3a). In this region the limestone was more fragmented, with open bedding planes infilled with red earth sediments and weathered material. This limestone had inverted resistivity values ranging from 100 to 300 Ωm. It is observable in Fig. 3a that most of the southern portion of the section had similar inverted resistivity values, suggesting that the unloading and weathering of the thinly bedded limestone extends to at least 21 m. On the southern half of the section, and at depths of greater than 5 m higher resistivity values ranging from ~ 500 up to 2,000 Ωm are observable presumably delineating zones of more compacted/less weathered thinly bedded limestone. A near vertical zone with an inverted resistivity of around 250 Ωm, in the south part of the image at about 170–185 m along the line, between two higher resistivity zones could indicate a fracture/weathered zone.

Two-dimensional resistivity-imaging section P2 (Fig. 4) runs parallel and 60 m to the east of line P1, and is 235 m long. The southern portion of the line transverses the thinly bedded limestone, while the northern portion traverses the eastern edge of the floodplain alluvium. This line is close to the boundary between the thinly bedded limestone and the massive limestone on the hill-slope (in the east). It is along this boundary that the tourist caves formed within the massive limestone unit. The RMS error for this resistivity model is 2.1 %, indicating a plausible resistivity image model.

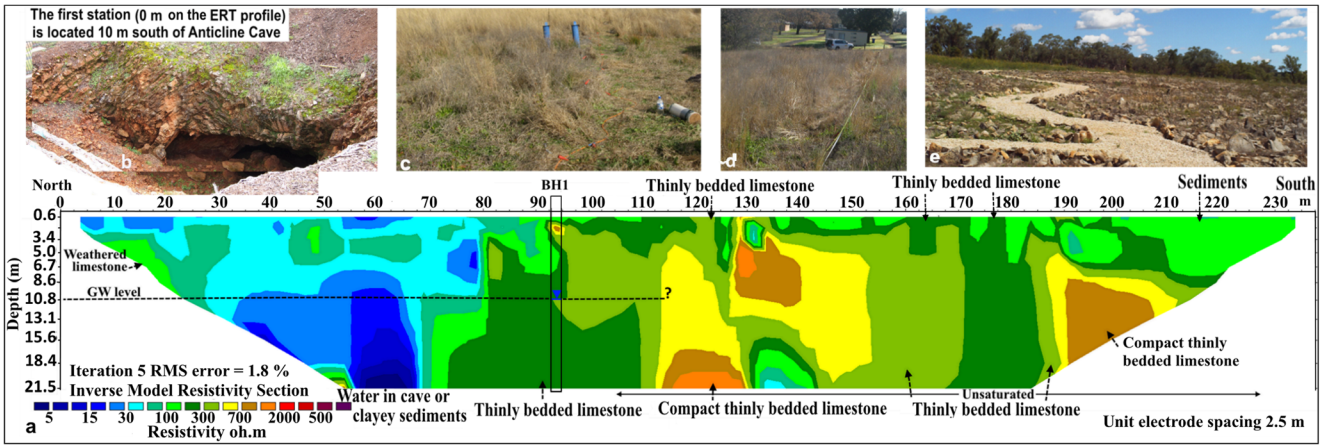

Fig. 3 **a** 2D resistivity-imaging section P1 measured over alluvium and thinly bedded limestone. The section is 235 m long and oriented north to south. The maximum effective depth of investigation was 21.5 m. The groundwater level (10.7 m deep; 298.3 m.a.s.l.) in **b** Anticline Cave and **c** the borehole BH1 was found to be very close to the top of the lowest resistivity anomalies (<20 Ωm) in the resistivity image. The southern part of the resistivity image was obtained at the outcrop of the thinly bedded limestone (**d** and **e**) at Fossil Trail

Line P2 (Fig. 4a) also shows a nearly vertical boundary 120 m along the section, with low resistivity values to the north (left; 0–120 m) over the alluvial sediments and high resistivity in the south (right; 120–235 m) overlies the thinly bedded limestone. In the northern part of the resistivity profile (0–120 m) and at a depth of 0–7 m the inverted resistivity values of 100–200 Ωm delineate the unsaturated medium- to coarse-grained alluvial sediments. The lowest inverted resistivity anomaly (<15 Ωm) at 62–75 m along the profile and at a depth of 13–21.5 m, in the northern part of the resistivity section could be either a cave filled with groundwater or clayey sediments. The southern half of the resistivity image over outcropping thinly bedded limestone has higher inverted resistivity values (400–2,000 Ωm). The highest inverted resistivity anomaly (>2,000 Ωm), a small vertical structure observed at 164 m and a depth of 5.5–9 m, because of its shape is interpreted as an air-filled cavity. Further work is required to verify this interpretation, and exclude the possibility of the anomaly being competent limestone.

Resistivity-imaging line P3 (Fig. 5) traverses the massive limestone, a lithological unit where significant caves have formed. This profile is located 45 m to the west of Cathedral Cave, and close to Lime Kiln Cave. This inverted resistivity section has an RMS error of 4.7 %, indicating a possibly valid solution. Within the section, the weathered limestone (100–500 Ωm), with possible sediment-filled joint networks and cavities, occurs in the upper 8 m of the northern side of the line, and to 21.5 m in the south. Competent limestone with inverted resistivity in the range of 500–2,500 Ωm is apparent north of 100 m along the line at depths 10 m below the ground surface.

Air-filled caves are discernible as high inverted resistivity anomalies (>2,500 Ωm) centered at 40 and 60 m along the profile in the vicinity of Mitchell Cave and Cathedral Cave.

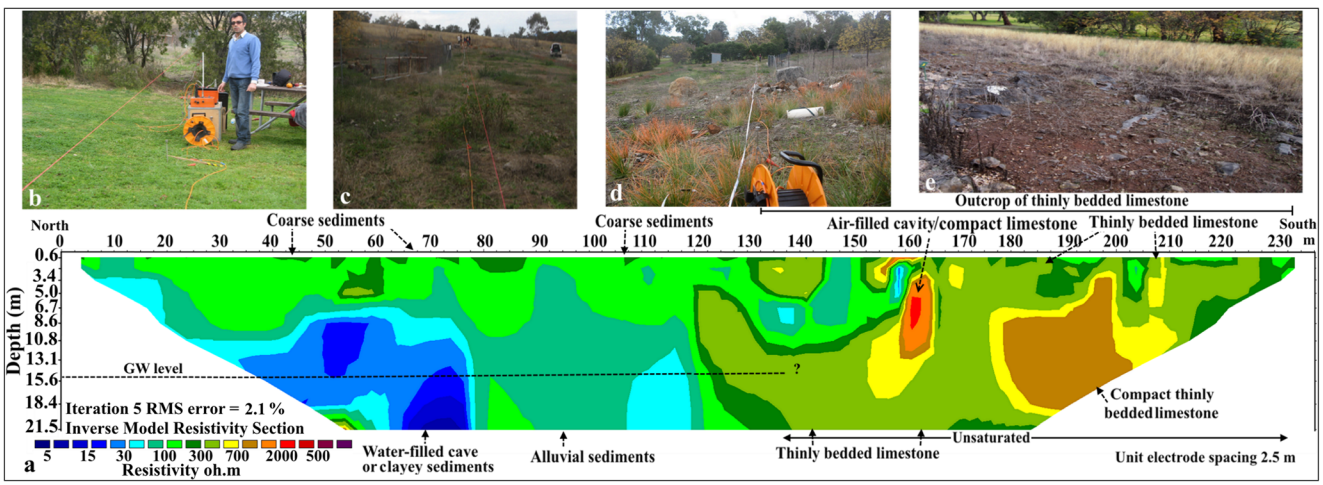

Fig. 4 **a** 2D resistivity-imaging section P2 measured over the thinly bedded limestone. It is parallel and to the east of profile P1. The survey line was 235 m long and oriented north to south. There were mostly alluvial sediments in the northern portion of the transect (**b**–**d**). **d** Photograph of the surficial coarse sediments. **e** Shows the outcrop of thinly bedded limestone in the southern portion of the imaging

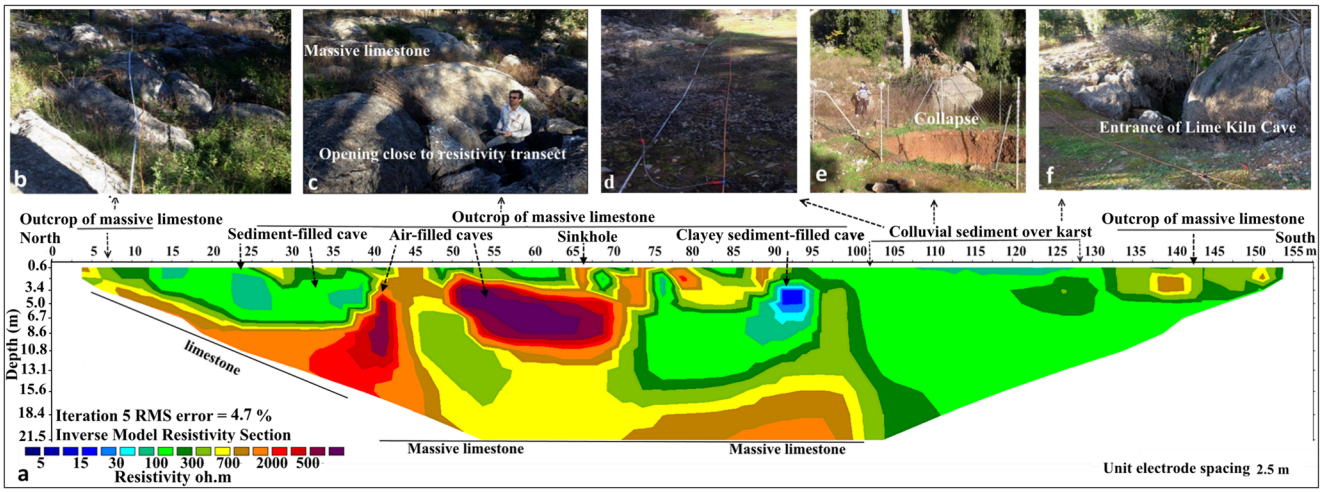

Fig. 5 Profile P3 **a** oriented north to south and located 60 m east of profile P2, over the karst system within the massive limestone. This profile is 45 m west of Cathedral Cave, and close to Lime Kiln Cave (see Fig. 1). **b** Outcrop of massive limestone along the left side of the resistivity-imaging section. **c** Sinkhole openings in the massive limestone. **d** Colluvial sediment close to the entrance of Lime Kiln Cave. **e** Collapse feature in the colluvial sediment over the karst system. **f** Entrance to Lime Kiln Cave

Figure 5b shows some openings/sinkholes close to this resistivity line, which are connected to known shallow caves. In the southern portion of profile P3, a clayey-sediment-filled cave with an inverted resistivity of ~ 30 Ωm is observable at 90–95 m at a depth of 3.5–7 m. At this site the groundwater level, as observed in the Well of Cathedral Cave, occurs at the depth of 24 m below the ground surface, thus the low resistivity anomaly is unlikely to be water filled.

The southern part of the resistivity imaging profile was carried out close to the entrance of Lime Kiln Cave (Fig. 5d). This karst passage overlies the northwest of the large McCavity Cave system, which is completely filled with groundwater. It is at a depth of more than 24 m, and it is therefore not observable in the resistivity image.

Water level analysis

Groundwater levels in the monitoring sites (Figs. 6, 7 and 8 and Table 3) in the karst system and the alluvium varied greatly according to the Bell River stage height during the monitoring interval 2010–2014, particularly during floods (early December 2010 (Fig. 7a,b), early March 2012, middle July 2012, and middle March 2014). Stream flow gauging station 421018 (NSW Office of Water Gauge) at Neurea is

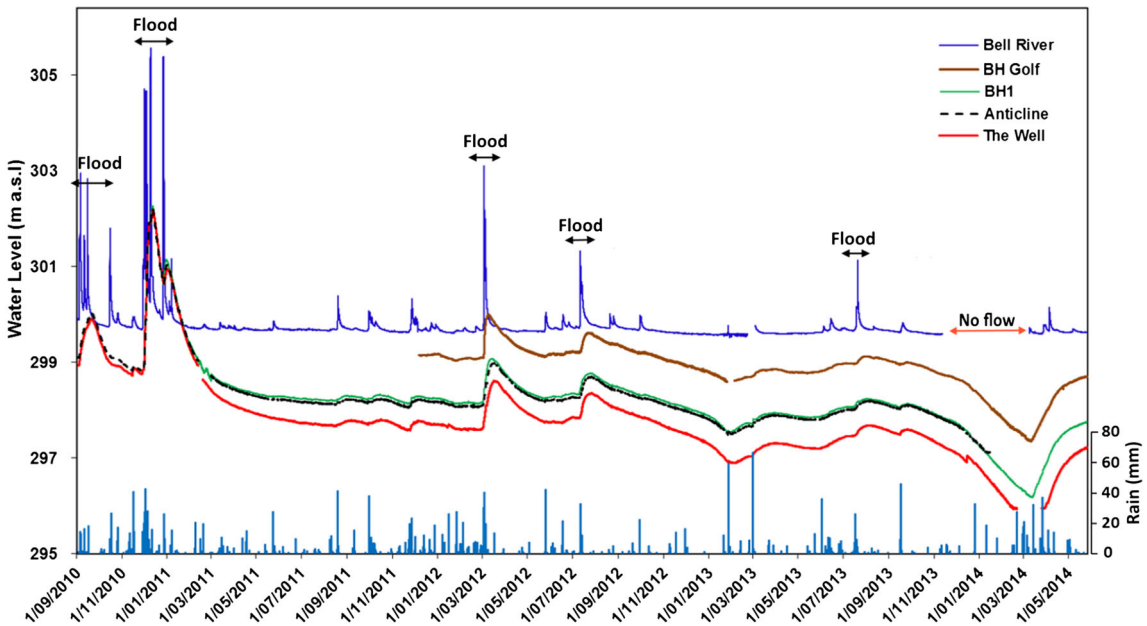

Fig. 6 Time series of surface-water and groundwater hydrographs. The rain data is daily rain and the water level data was recorded every 15 min. The Well in Cathedral Cave, Anticline Cave, and borehole BH1 are all in the karst, whereas borehole *BH Golf* is in the alluvium

Fig. 7 **a**–**b** Photos show flooding in the Bell River in December 2010, **c** high GW level in Cathedral Cave, during the floods of December 2010, **d**–**e** shows no-flow in the Bell River during drought period December 2013–February 2014, **f** shows flow in the river on 16th March 2014. The decline of GW levels is observed in Anticline Cave (**g**) and The Well (**h**) during no-flow in the river

located 5 km upstream of the caves. To allow comparison with the borehole and cave water level measurements, and to provide a proxy for stream flow at location "S" (Fig. 1a), 12.769 m is subtracted from stream flow gauge 421018 in Figs. 6 and 8.

Table 2 presents the rainfall data for Wellington, and the months with flooding are highlighted in italics. The rainfall and streamflow data show that there is a complex relationship between rainfall intensity, proximity of rainfall to the gauging stations, past wetting of the system, and river and groundwater levels. Two examples highlight aspects of the complex relationship. Annual rainfall was similar in 2011 and 2012, yet there was no significant rise in groundwater level in 2011 in comparison to 2012, which had a 1 m rise in early March 2012 and a 0.6 m rise in mid-July 2012 (Fig. 6). It is notable that November 2011 was a wet month (108.3 mm) yet there were only small rises in the river and groundwater levels associated with higher than average rainfall. By contrast, a significant flood peak is observable in July 2012 when just 55.4 mm of rainfall was recorded for the month at Wellington. Floodwater in the Bell River depends on the rainfall and the antecedent soil moisture in the catchment area (1,248 km^2). March 2014, was a wet than average month, but occurred after a period of no flow in the Bell River adjacent to Wellington Cave Reserve. Figure 6 shows a small response in the Bell River stage due to this rainfall. However, this small rise in the river stage resulted in renewed flow adjacent to the area, and led to groundwater level recovery.

The largest floods were associated with intense rainfall on 28 November 2010 and 1 December 2010. Streamflow in the Bell River at the gauging station located upstream of the study area increased from around 100 ML/day on 28 November 2010 to 26,600 ML/day on 1 December 2010 and to 26,240 ML/day on 4 December 2010. Figure 6 shows the groundwater response in the boreholes and caves as the flood moves through the study reach of the Bell River. The shallow alluvial aquifer adjacent to the river responded quickly to the increases in river stage. Groundwater levels in Anticline Cave, and The Well responded to the 1st and 4th of December 2010 flood peaks within 65 ± 4 and 85 ± 4 h, respectively (Fig. 8a and

Fig. 8 Groundwater response to flooding in the Bell River in **a** December 2010, **b** March 2012, **c** July 2012 and **d** to renewed flow in the river in March 2014. The groundwater level at The Well was below the level of the logger during February–March 2014 and data are extrapolated. The water level data were recorded every 15 min

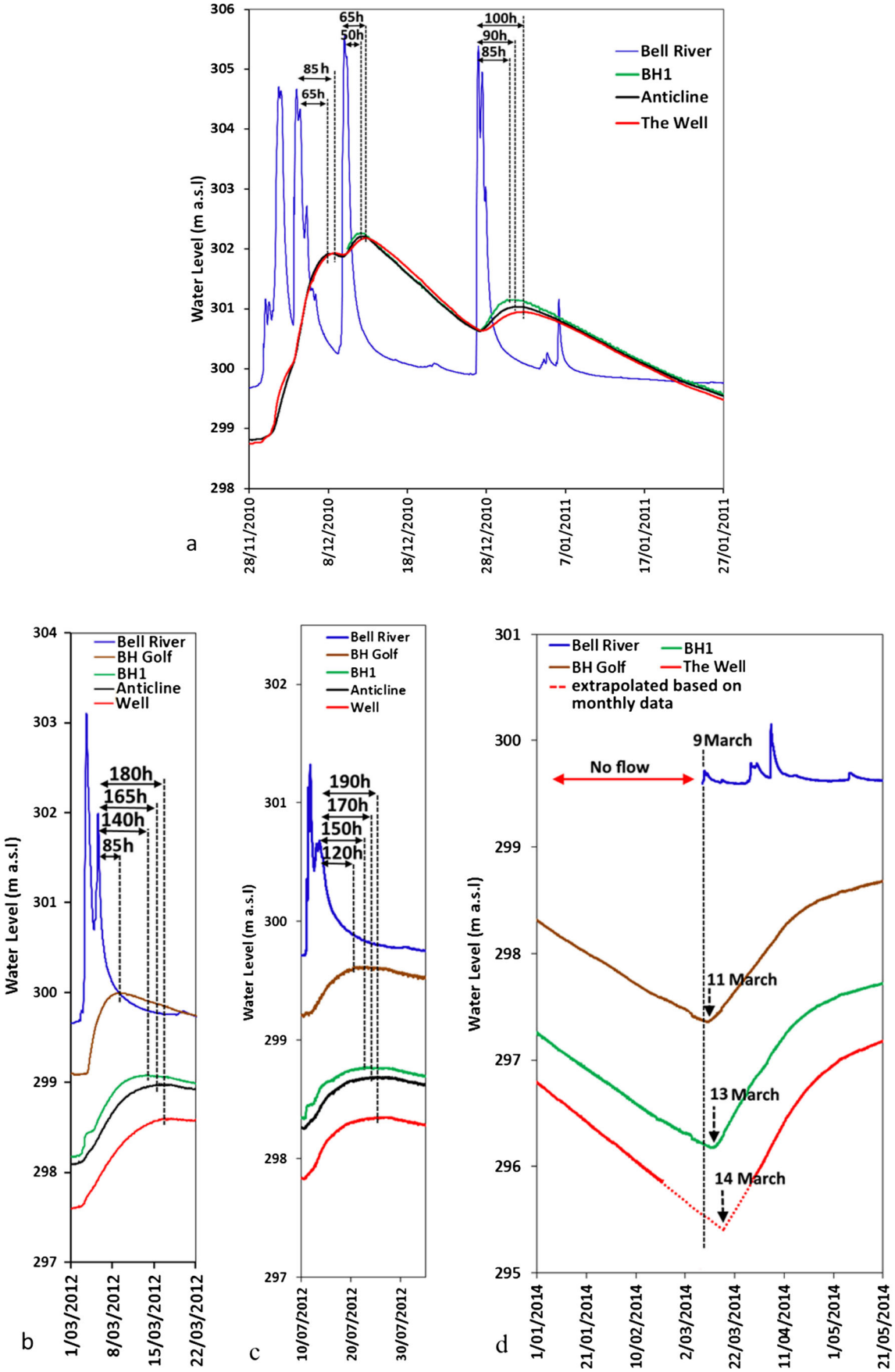
a
Water Level (m a.s.l)
306
305
304
303
302
301
300
299
298
65h
50h
85 h
65h
100h
90h
85h
Bell River
BH1
Anticline
The Well
28/11/2010
8/12/2010
18/12/2010
28/12/2010
7/01/2011
17/01/2011
27/01/2011
b
Water Level (m a.s.l)
304
303
302
301
300
299
298
297
Bell River
BH Golf
BH1
Anticline
Well
180h
165h
140h
85h
1/03/2012
8/03/2012
15/03/2012
22/03/2012
c
Water Level (m a.s.l)
302
301
300
299
298
297
Bell River
BH Golf
BH1
Anticline
Well
190h
170h
150h
120h
10/07/2012
20/07/2012
30/07/2012
d
Water Level (m a.s.l)
301
300
299
298
297
296
295
Bell River
BH1
BH Golf
The Well
extrapolated based on monthly data
No flow
9 March
11 March
13 March
14 March
1/01/2014
21/01/2014
10/02/2014
2/03/2014
22/03/2014
11/04/2014
1/05/2014
21/05/2014

Table 2 Monthly and annual rain (mm) in the study area, Wellington, NSW—BOM Station WELLINGTON (AGROWPLOW) (Australian Government Bureau of Meteorology 2015)

Year	Jan	Feb	Mar	Apr	May	Jun	Jul	Aug	Sep	Oct	Nov	Dec	Annual
2010	26.2	117.0	111.8	62.6	50.7	34.6	94.0	83.2	72.6	82.1	*159.2*	*179.7*	1073.7
2011	26.4	60.0	34.0	37.2	46.4	15.8	12.8	77.6	65.6	41.3	108.3	68.0	593.4
2012	101.1	84.2	*125.6*	6.9	56.2	53.4	*55.4*	8.2	34.4	6.4	43.8	5.6	581.2
2013	84.2	21.2	100	6.2	20.6	103.6	55.1	7.6	62.2	5.3	21.5	42.2	529.7
2014	31.4	58.6	*157.8*	44.6	18.2	63.3	45.7	24.3	22.7	23.2	25.0	61.8	576.6

Months with flooding are highlighted in *italics*

Table 3). During this flood, there was a 5 m (from 299.7 to 304.7 m.a.s.l.) rise of water level in the river, the groundwater level increased continuously 3.07 m (from 298.83 to 301.9 m.a.s.l.) in both Anticline Cave and The Well. For the flood 9–11 December 2010 (Fig. 8a and Table 3), the river water level rise was 5.20 m, and the groundwater levels rose in BH1, Anticline Cave and at The Well by 0.37, 0.31 and 0.28 m and with delays of 50 ± 4 h, 55 ± 4 h, and 65 ± 4 h, respectively. In this study, the flood peaks in the river are compared with the peaks in groundwater level.

The groundwater level in The Well (in Cathedral Cave) is normally around 25 and 35 cm lower than in the Anticline Cave and BH1, with 205 m and 260 m distance between them, respectively, but this difference is less than 10 cm during the 2010 flood.

Rainfall of 159 mm in November and 180 mm in December 2010 caused large floods in the Bell River. Floodwaters spread over the overbank alluvium along the Bell River and a sharp rise in groundwater levels within the alluvial aquifer and karst system were observable. Groundwater levels also rose at BH1, Anticline cave and at The Well in response to the flooding on the 26–28 December 2010 (stage increase 5.5 m) with a rise of 0.52, 0.40 and 0.31 m and with a delays of 85 ± 4 h, 90 ± 4 h, and 100 ± 4 h, respectively (Fig. 8a and Table 3).

Observable in the hydrograph (Fig. 6), the rising limbs of the groundwater level during a flood are closer to vertical compared to the falling limbs, particularly during the 2010 floods. Groundwater level in the karst system was higher than the water level in the river during 6–8 December 2010, 12–25 December 2010 and 1–20 January 2011, which shows a reversal of the hydraulic gradient from the aquifer to the river, and a shift from a losing to a gaining river.

Flooding (~3 m stage rise) in early March 2012 (Fig. 8b and Table 3) resulted in a noticeable rise (1 m) in the groundwater levels within the caves and alluvium. At BH Golf (350 m east of the river, located in the alluvial aquifer) the groundwater level rose 0.90 m after 85 ± 5 h. After the flood, the groundwater level at BH Golf was 8 cm higher than the river water level for a weeklong period. After the March 2012 flood, the groundwater level continued to rise in the Karst monitoring sites (Fig. 8b and Table 3): 0.90 m in BH1 (located 710 m east of the river) after 140 ± 10 h, 0.90 m in Anticline Cave (located 670 m east of the river and 100 m north of BH1) after 160 ± 10 h, and 1.0 m in The Well (located 820 m east of the river) after 180 ± 10 h.

Flooding of the Bell River (1.5 m rise) in mid July 2012 (Fig. 8c and Table 3) increased the groundwater level by 0.51 m in BH Golf after 120 ± 10 h, by 0.47 m in BH1 after 150 ± 10 h, by 0.45 m in Anticline Cave after 170 ± 10 h, and by 0.51 m at The Well after 190 ± 10 h.

There was no- flow in the Bell River (Figs. 6, 7d,e, and 8c) in the reach of the study area from mid-December 2013 to early-March 2014. Groundwater level responded sharply to this loss of surface-water flow and experienced a noticeable decrease of 1.4 m in the alluvial aquifer (BH Golf) and 1.7 m in the karst aquifer (BH1, Anticline Cave and The Well,

Table 3 Flood events in the Bell River and groundwater response

Flood	Bell River		BH Golf (Alluvial)			BH1 (Karst)			Anticline (Karst)			The Well (Karst)		
Date	WL peak m.a.s.l.	WL rise (m)	WL peak m.a.s.l.	WL rise (m)	Lag time (h)	WL peak m.a.s.l.	WL rise (m)	Lag time (h)	WL peak m.a.s.l.	WL rise (m)	Lag time (h)	WL peak m.a.s.l.	WL rise (m)	Lag time (h)
1–5 Dec 2010	304.60	4.90	–	–	–	–	–	–	301.93	3.07	65 ± 4	301.93	3.07	85 ± 4
9–10 Dec 2010	305.50	5.20	–	–	–	302.26	0.37	50 ± 4	302.21	0.31	55 ± 4	302.18	0.28	65 ± 4
26–28 Dec 2010	305.90	5.5	–	–	–	301.14	0.52	85 ± 4	301.03	0.40	90 ± 4	300.94	0.31	100 ± 4
3–6 March 2012	303.00	3.43	299.61	0.91	85 ± 5	299.07	0.90	140 ± 10	298.98	0.90	160 ± 10	298.6	1.00	180 ± 10
10–15 Jul 2012	301.30	1.61	299.7	0.51	120 ± 10	299.00	0.47	150 ± 10	298.68	0.45	170 ± 10	298.12	0.51	190 ± 10

A strong correlation between the peaks in the river during flooding and the groundwater level peaks is observed

Fig. 8g,h). Renewed flow in Bell River on 9 March 2014 saw the groundwater levels rapidly respond within hours: 50 ± 10 h delay in BH Golf, 90 ± 10 h delay in BH1, and 120 ± 10 h delay in the Well (Fig. 8c). In the month following the renewed flow in the Bell River (Figs. 7f and 8d) the groundwater level rose by 0.90 m in BH Golf, located in the alluvial aquifer, and 1.15 m in BH1, located in the karst aquifer.

Chloride concentrations

The groundwater monitoring sites and the Bell River were sampled at monthly intervals between January and July 2014 for chloride concentrations. As there was no-flow in the Bell River, in the reach of Wellington Cave Reserve, from December 2013 to mid-March 2014 (Figs. 6 and 7d,e), river-water samples were collected upstream, 1,000 m south, in January and February 2014. The chloride content (Fig. 9) in the river was high (about 85 mg/L) during low-flow conditions that occurred in January through February 2014. This is expected due to more evaporation and a greater contribution from salinity sources in the soil and alluvial sediments (Dragovich and Dominis 2008; Haron and Dragovich 2010) in summer. Renew flow in the river occurred on 9 March 2014 and gradually recharged the groundwater level (Fig. 8d). The first floodwater in the river showed a high value of Cl (83 mg/L) in March 2014, which decreased to 75 mg/L in April and stabilised in May. The chloride concentration in the river decreased sharply to 58 and 46 mg/L due to more dilution in June and July, respectively.

The chloride content in both the alluvial and karst aquifer showed a decrease from January to late February when there was no recharge from the river, and then showed an increase after the flow event in the river from March to June 2014. The groundwater chloride concentrations, particularly in WA5, WA1, WA3 and WA2 located in the alluvium with distance 40–200 m from the river, exhibited higher chloride values (ranges 72–77 mg/L) from March to June 2014, suggesting recharge with river water high in chloride (83–75 mg/L) from March to May. The groundwater chloride concentrations exhibited a sharp decrease at the end of July. This decrease in chloride concentration in groundwater samples can be interpreted as a response to recharge from the river water, which had lower chloride content (58 and 46 mg/L from June and July). Water samples from Anticline, BH1 and The Well (Cathedral Cave) within the karst showed around 5 mg/L decrease in July. The change in chloride content can be interpreted as a signal of direct hydraulic connectivity between the river and aquifer systems in the study area.

Hydraulic gradient and conceptual hydrogeological model

According to the surface-water and groundwater level data, the hydraulic gradient in the reach of Wellington Caves Reserve is predominantly from the Bell River (surface water), across the alluvium towards the limestone. Figure 10 shows the groundwater flow direction in the study area during different periods. When there is low flow in the Bell River, groundwater flows from the south-west to north-east (Fig. 10a). The high hydraulic gradient from the Bell River towards the adjacent alluvial aquifer was observed on two occasions, during flooding (example early March 2012) and during the first months of renewed flow in the river after a dried period (example March 2014), when the head difference between the surface water and groundwater is at its maximum (Figs. 6, 8d, and 10b). The maximum hydraulic gradient between the river and BH Golf (350 m east of the river) was 0.0125 in March 2012. In March 2014 the head gradients from the river to WA2 (200 m east of the river) and BH Golf were 0.0125 and 0.0072, respectively. The head gradients then gradually decreased through to the end of May when they were measured to be 0.0065 and 0.0031, respectively. In contrast, the minimum head gradient, nearly zero, between the river and the groundwater in the alluvium occurred several days after the flood recession such as 23–30 September 2010 and 18–25 March 2012 (Fig. 6). The head gradient shifted from the groundwater towards the river (Figs. 8a and 10c) for the short periods of 6–8 December 2010, 12–25 December 2010 and 1–20 January 2011.

The hydraulic gradient in the alluvial aquifer from west to east between WA2 and BH1 has been mostly around 0.0012. The head gradient in the alluvial is 0.0009 from south to north between BH Golf and WA2. Within the karst aquifer, the

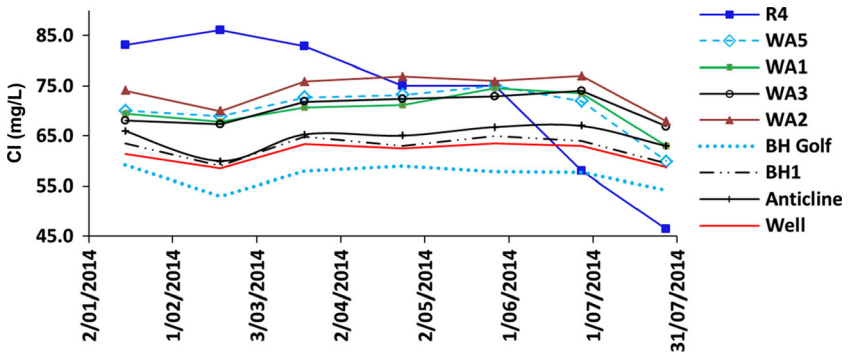

Fig. 9 Comparison of chloride concentration in surface water and groundwater at monitoring sites in the study area, Wellington, NSW

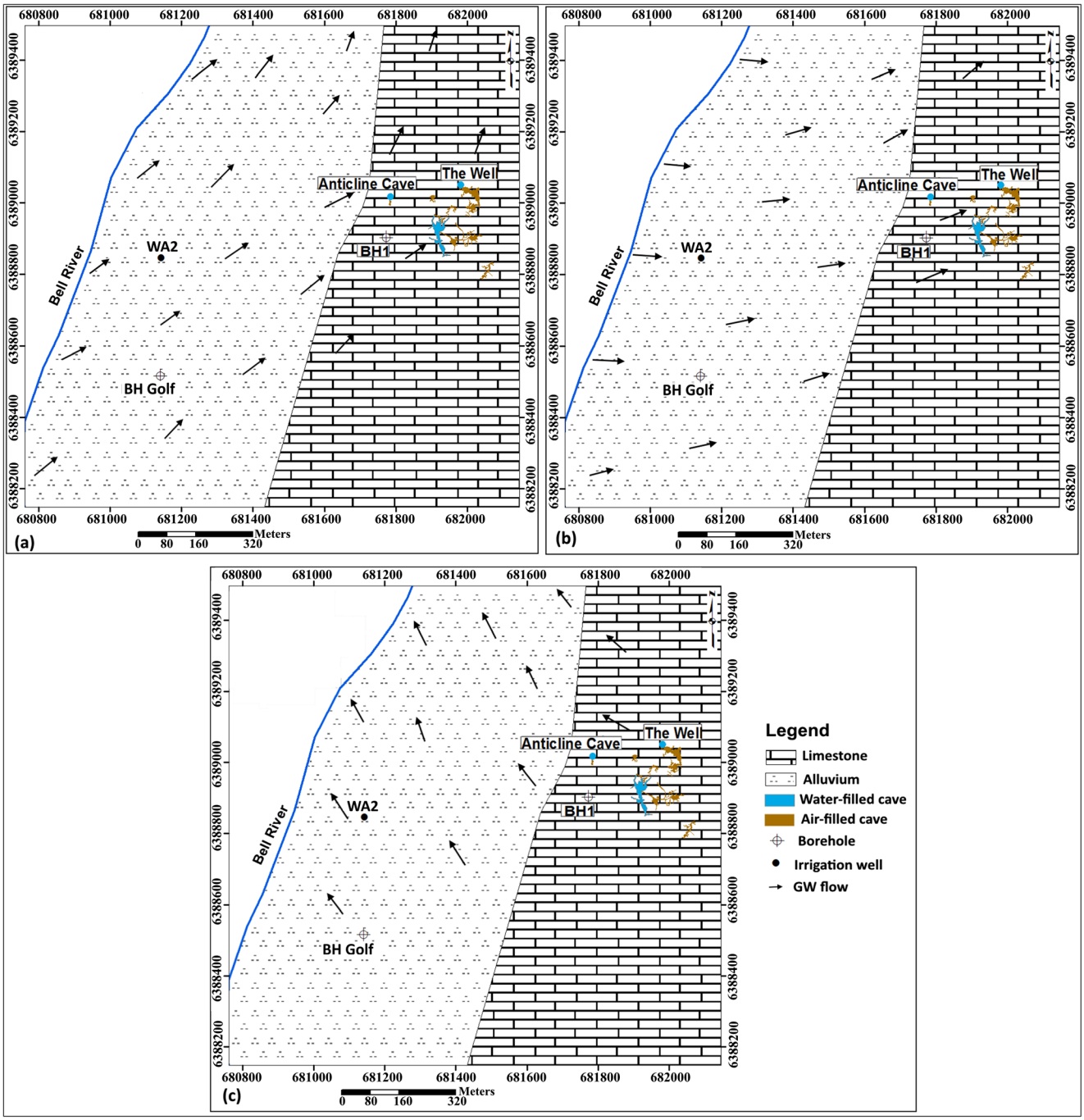

Fig. 10 **a** Inferred general groundwater flow direction in the study area during base flow and low flow in the Bell River, **b** groundwater flow direction during flooding of the Bell River, and **c** reverse groundwater flow direction from the karst-alluvial aquifer to the Bell River during a short period (around 40 days), only after the flood in December 2010. Groundwater level data for boreholes *BH1* and *BH Golf*, *Anticline Cave* and *The Well* were recorded at 15-min intervals using Solinst loggers 2010–2014. This data was supplemented by monitoring water levels at three irrigation bores (WA2, WA3, WA5) in 2013–2014

hydraulic gradient between BH1 and Anticline is 0.0013 and between Anticline and The Well is 0.0016 during base flow conditions. When there is no-flow in the river, like February–early March 2014, the hydraulic gradient was observed nearly similar 0.0022, from south to north between WA2 and WA3 (2130 in the north of the Wellington Caves), and between The Well and WA3. This gradient decreased to 0.0014 in mid-April 2014 after 1 month of flow in the river.

When there is flooding in the river, the hydraulic gradient (Fig. 10b) is mostly from west (from the river) to east (aquifer), which results in more recharge to the aquifer system and the groundwater level rises significantly. In contrast, when there is

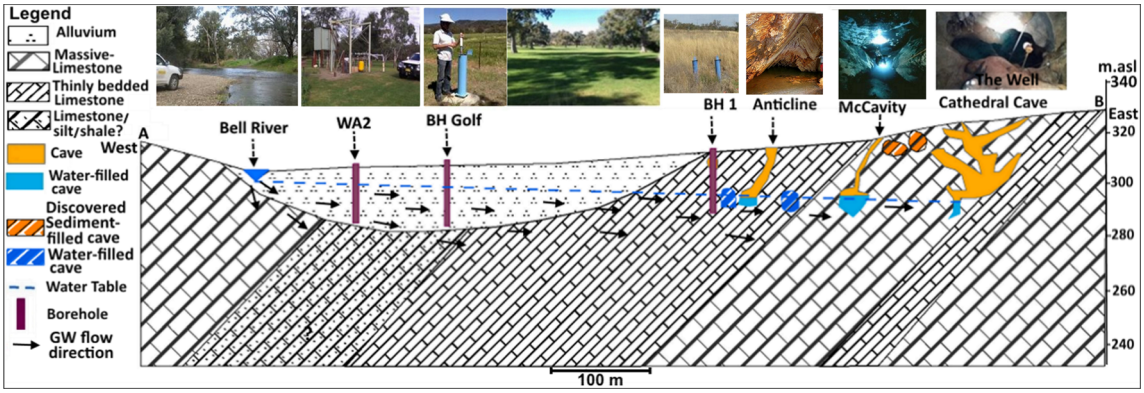

Fig. 11 Conceptual hydrogeological transect model (west to east) from Wellington Caves, alluvium (*BH Golf*) to Bell River (during losing conditions)

no-flow in the river, the hydraulic gradient is 0.0022 from south to north in the alluvium and karst. Therefore, the hydraulic gradient becomes predominant from south to north during drought periods. After extensive flooding, where floodwaters cover the width of the valley as occurred in December 2010, the hydraulic gradient is reversed to the northwest (Fig. 10c), from the aquifer to the river, for a short period (6–8 December 2010, 12–25 December 2010 and 1–20 January 2011).

Annual groundwater withdrawals of 1,370 ML/year from the alluvial aquifer contribute to a decline in the groundwater level (1.5 m), particularly during periods of drought. The groundwater levels in the alluvial aquifer and karst system recover rapidly as soon as there is a continuous flow in the Bell River in the reach of Wellington Cave Reserve, once river losses exceed the rate of groundwater discharge.

The conceptual model developed from the collection and interpretation of the geophysical, hydrogeological and chloride datasets in the study area is shown in Fig. 11. The sections show the conceptual hydrogeological transect model (west to east) from the Bell River, across the alluvium to the Wellington Caves Reserve in the limestone. The geophysical resistivity surveys mapped the location of possible new water-filled, sediment-filled and air-filled caves in the study area.

For most of the period studied, the groundwater level in the shallow alluvial aquifer was lower than the Bell River, and the river is losing and recharging the alluvial aquifer (Figs. 10a,b and 11). During losing conditions, the groundwater level in the shallow alluvial aquifer is significantly lower than the surface-water level in the river, and the groundwater level in the Anticline Cave within the karst system is lower than the alluvial aquifer. The groundwater level in Anticline and BH1 is generally higher than the groundwater level in The Well (which is the deepest part of Cathedral Cave). Therefore, the hydraulic gradient in this reach of the Bell River adjacent to Wellington Caves Reserve is predominantly from the Bell River (surface water) across the alluvium towards the limestone. Consequently, any surface-water recharge on the alluvial aquifer will flow towards the karst system.

Conclusion

This study presents the results on the combined use of 2D resistivity imaging, water level analysis, and chloride measurements to improve current knowledge about exchanges between the Bell River and the adjacent alluvial and karst aquifers at Wellington Caves, NSW Australia. The data show that the groundwater recharge was dominated by river losses throughout most of the year. Only during the recession after major floods did the Bell River switch to gaining for small periods.

The resistivity imaging (Figs. 3a, 4a, and 5a) delineated potential new karstic cavities within the Garra Limestone. Potential air-filed cavities were delineated by >2,500 Ωm anomalies, water-filled caves are likely in zones where the resistivity was <15 Ωm, and sediment-filled cavities where delineated by conduit and cave shaped anomalies with inverted resistivity readings in the 30–150 Ωm range. From the resistivity images, it can be inferred that there are likely cavities that can act as potential pathways for groundwater flow, connecting Wellington karst aquifer with the alluvial aquifer and the Bell River.

Groundwater level response to river stage varies across the floodplain. Groundwater levels in the karst caves (The Well within Cathedral and Anticline) and boreholes are highly responsive to flooding and no-flow in the Bell River. Comparing the peaks in the groundwater levels with the peaks in the adjacent river (early December 2010 (Fig. 8a), early March 2012 (Fig. 8b), middle July 2012, and middle March 2014 (Fig. 8c), shows a strong correlation between flooding and the groundwater levels. This confirms the hydraulic connection between the Bell River and groundwater within alluvial and karst systems in the study area. The water level analysis is further supported by insights from the chloride concentration measurements (Fig. 9). This shows a losing river (Figs. 10a,b and 11) with high chloride (83–75 mg/L) from March to May recharging into the aquifers which slightly increased chloride concentration in the groundwater. The river chloride concentration dropped significantly to 58 and 46 mg/

L between June and July 2014. The fresh river water recharging into the aquifers diluted the groundwater and resulted in lower chloride values of the groundwater at the end of July (Fig. 9).

Groundwater, in the study area during moderate to low flow in the Bell River, generally flows from south-west to north-east (Fig. 10a). When there is flooding in the river, the hydraulic gradient (Fig. 10b) is mostly from west (from the river) to east (alluvial and karst aquifers), resulting in more recharge to the aquifers and the groundwater level rose significantly. Only after the largest flood observed did the hydraulic gradient temporally reverse, and the Bell River switched to gaining (Fig. 10c).

During the period of no-flow in the Bell River, the water table declined rapidly in both the karst and alluvial aquifers, and the water table gradient increased to 0.0022 from south to north (Figs. 7d,e and 8d), which indicates that groundwater input from the south of the caves complex does not balance the groundwater outflows to the north. An alternative interpretation is that groundwater extractions (with 1,370 ML annually) to the north of the caves are causing a decline in the water table that extends up the gradient. This has important implications for the protection of the Wellington tourist caves and also for water resources management of this area. Further research is required to separate which process is causing the significant declines in groundwater levels within the Wellington Caves Reserve during periods of no-flow in the Bell River.

Acknowledgements Bore BH1 was installed utilising funding from the Federal Government NCRIS Groundwater Infrastructure Program. Funding was also received from the National Centre for Groundwater Research and Training (NCGRT), and help was provided by Dr. Gabriel C Rau, Dr Hoori Ajami, Mr. Amir Abas Hayati, the Wellington Council and staff at Wellington Caves.

References

Acworth RI, Dasey GR (2003) Mapping of the hyporheic zone around a tidal creek using a combination of borehole logging, borehole electrical tomography and cross-creek electrical imaging, New South Wales, Australia. Hydrogeol J 11(3): 368–377. doi:10.1007/s10040-003-0258-4

Allison G, Hughes M (1978) The use of environmental chloride and tritium to estimate total recharge to an unconfined aquifer. Soil Res 16(2):181–195. doi:10.1071/SR9780181

Andersen MS, Acworth RI (2009) Stream-aquifer interactions in the Maules Creek catchment, Namoi Valley, New South Wales, Australia. Hydrogeol J 17:2005–2021. doi:10.1007/s10040-009-0500-9

Anderson AN, McKenzie DC, Friend JJ (1999) SOILpak for dryland farmers on the red soil of Central Western NSW. NSW Agriculture. http://www.dpi.nsw.gov.au/content/agriculture/resources/soils/guides/soilpak/central-west. Accessed 5 Aug 2015

Australian Government Bureau of Meteorology (BOM) (2015) Latest weather observations for Parramatta. http://www.bom.gov.au/products/IDN60801/IDN60801.94723.shtml. Accessed 1 Feb 2015

Bailly-Comte V, Jourde H, Pistre S (2009) Conceptualization and classification of groundwater–surface water hydrodynamic interactions in Karst watersheds: case of the Karst watershed of the Coulazou River (southern France). J Hydrol 376(3–4):456–462. doi:10.1016/j.jhydrol.2009.07.053

Bakalowicz M (2005) Karst groundwater: a challenge for new resources. Hydrogeol J 13(1):148–160. doi:10.1007/s10040-004-0402-9

Binley A, Kemna A (2005) DC resistivity and induced polarization methods. In: Rubin Y, Hubbard S (eds) Hydrogeophysics. Water and Science Technology Library, Springer, Dordrecht, The Netherlands, pp 129–156

Blyth AJ, Jex C, Baker A, Khan SJ, Schouten S (2014) Contrasting distributions of glycerol dialkyl glycerol tetraethers (GDGTs) in speleothems and associated soils. Org Geochem 69:1–10. doi:10.1016/j.orggeochem.2014.01.013

Bonacci O (2015) Surface waters and groundwater in Karst. In: Stevanović Z (Ed) Karst Aquifers: characterization and engineering. Professional Practice in Earth Sciences. Springer, Heidelberg, Germany, pp 149–169

Bonacci O, Ljubenkov I, Roje-Bonacci T (2006) Karst flash floods: an example from the Dinaric karst (Croatia). Nat Hazards Earth Syst Sci 6(2):195–203. doi:10.5194/nhess-6-195-2006

Brown AL, Martin JB, Screaton EJ, Ezell JE, Spellman P, Gulley J (2014) Bank storage in Karst aquifers: the impact of temporary intrusion of river water on carbonate dissolution and trace metal mobility. Chem Geol 385:56–69. doi:10.1016/j.chemgeo.2014.06.015

Carroll D, Hathaway JC (1953) Clay minerals in a limestone soil profile. Second National Conference on Clays and Clay Minerals, Columbia, MO, October 1953, pp 171–182

Chatterton BDE, Johnson BD, Campbell KSW (1979) Silicified lower Devonian trilobites from New South Wales. Palaeontology 22:799–837

Cook KL, Van Nostrand RG (1954) Interpretation of resistivity data over filled sinks. Geophysics 19(4):761–790. doi:10.1190/1.1438048

Cox MH, Su GW, Constantz J (2007) Heat, chloride, and specific conductance as ground water tracers near streams. Ground Water 45(2): 187–195. doi:10.1111/j.1745-6584.2006.00276.x

Dahlin T (2001) The development of DC resistivity imaging techniques. Comput Geosci 27(9):1019–1029. doi:10.1016/S0098-3004(00)00160-6

Dahlin T, Zhou B (2004) A numerical comparison of 2D resistivity imaging with 10 electrode arrays. Geophys Prospect 52(5):379–398. doi:10.1111/j.1365-2478.2004.00423.x

Dawson L (1985) Marsupial fossils from Wellington Caves, New South Wales: the historic and scientific significance of the collections in the Australian Museum, Sydney. Rec Aust Mus 37(2):55–69. doi:10.3853/j.0067-1975.37.1985.335

Dey A, Morrison H (1979) Resistivity modelling for arbitrarily shaped two-dimensional structures. Geophys Prospect 27:106–136

Dragovich D, Dominis M (2008) Dryland salinity and rainfall patterns: a preliminary investigation in central west New South Wales (Australia). Land Degrad Dev 19(5):564–573. doi:10.1002/ldr.866

Dubois C, Quinif Y, Baele J-M, Dagrain F, Deceuster J, Kaufmann O (2014) The evolution of the mineralogical and petrophysical properties of a weathered limestone in southern Belgium. Geol Belg 17:1–8

Freeze RA, Cherry JA (1979) Groundwater. Prentice Hall, Englewood Cliffs, NJ

Greenfield RJ, Lavin PM, Parizek RR (1976) Geophysical methods for location of voids and caves. Proceedings of the Anaheim Symposium, Anaheim, CA, December 1976, IAHS, Wallingford, UK

Gulley J, Martin JB, Screaton EJ, Moore PJ (2011) River reversals into Karst springs: a model for cave enlargement in

eogenetic Karst aquifers. Geol Soc Am Bull 123(3–4):457–467. doi:10.1130/b30254.1

Habberjam GM (1969) The location of spherical cavities using a tripotential resistivity technique. Geophysics 34:780–784. doi:10.1190/1.1440049

Haron M, Dragovich D (2010) Climatic influences on dryland salinity in central west New South Wales, Australia. J Arid Environ 74(10): 1216–1224. doi:10.1016/j.jaridenv.2010.04.014

Harvey RW, George LH, Smith RL, LeBlanc DR (1989) Transport of microspheres and indigenous bacteria through a sandy aquifer: results of natural- and forced-gradient tracer experiments. Environ Sci Technol 23(1):51–56. doi:10.1021/es00178a005

Hem JD (1985) Study and Interpretation of the chemical characteristics of natural water, 3rd edn. US Geological Survey, Reston, VA

Ivkovic KM (2009) A top-down approach to characterise aquifer–river interaction processes. J Hydrol 365(3–4):145–155. doi:10.1016/j.jhydrol.2008.11.021

Johnson BD (1975) The Garra formation (Early Devonian) at Wellington, NSW. J Proc R Soc NSW 108(December):111–118

Kaufman WJ, Orlob GT (1956) An evaluation of ground-water tracers. EOS Trans Am Geophys Union 37(3):297–306. doi:10.1029/TR037i003p00297

Kaufmann O, Deceuster J (2014) Detection and mapping of ghost-rock features in the Tournaisis area through geophysical methods: an overview. Geol Belg 17(1):17–26

Kaufmann G, Romanov D (2009) Geophysical investigation of a sinkhole in the northern Harz foreland (North Germany). Environ Geol 58(2):401–405. doi:10.1007/s00254-008-1598-0

Kaufmann O, Deceuster J, Quinif Y (2012) An electrical resistivity imaging-based strategy to enable site-scale planning over covered palaeokarst features in the Tournaisis area (Belgium). Eng Geol 133–134:49–65. doi:10.1016/j.enggeo.2012.01.017

Keshavarzi M, Graham P, Baker A, Kelly BF, Andersen M, Rau G, Acworth RI, Smithson A (2014) Understanding river–groundwater interactions in a Karst system, Wellington, NSW. Presented at "Sustainable Australia". Australian Earth Science Convention 2014, Newcastle, Australia, 7–10 July 2014. http://aesc2014.gsa.org.au/assets/Various-reg-partner-opp-workshop-summ-/AESC-Abstract-Proceedings.pdf. Accessed 20 Feb 2016

Kim J-H, Yi M-J, Cho S-J, Son J-S, Song W-K (2006) Anisotropic Crosshole resistivity tomography for ground safety analysis of a high-storied building over an abandoned mine. J Environ Eng Geophys 11(4):225–235. doi:10.2113/jeeg11.4.225

Leucci G, De Giorgi L (2005) Integrated geophysical surveys to assess the structural conditions of a Karstic cave of archaeological importance. Nat Hazards Earth Syst Sci 5(1):17–22. doi:10.5194/nhess-5-17-2005

Lindsey BD, Berndt MP, Katz BG, Ardis AF, Skach KA (2009) Factors affecting water quality in selected carbonate aquifers in the United States, 1993–2005. US Geol Surv Sci Invest Rep 2008-5240, 117 pp

Loke MH (1999) Electrical imaging surveys for environmental and engineering studies: a practical guide to 2-D and 3-D surveys. http://www.abem.se/. Accessed November 2016

Loke MH, Barker RD (1995) Least-squares deconvolution of apparent resistivity pseudosections. Geophys 60(6):1682–1690. doi:10.1190/1.1443900

Loke MH, Acworth I, Dahlin T (2003) A comparison of smooth and blocky inversion methods in 2D electrical imaging surveys. Explor Geophys 34(3):182–187. doi:10.1071/EG03182

Loke MH, Chambers JE, Rucker DF, Kuras O, Wilkinson PB (2013) Recent developments in the direct-current geoelectrical imaging method. J Appl Geophys 95:135–156. doi:10.1016/j.jappgeo.2013.02.017

Mawson R, Talent JA, Bear VC, Benson DS, Brock GA, Farrell JR, Hyland KA, Pyemont BD, Sloan TR, Sorentino L, Stewart MI, Trotter JA, Wilson GA, Simpson AG (1988) Conodont data in relation to resolution of stage and zonal boundaries for Devonian of Australia. In: McMillan NJ, Embry AF, Glass DJ (eds) Devonian of the world: Proceedings of the Second International Symposium on the Devonian System, Calgary, Canada. CSPG Spec Publ 14(3): 485–527

Musgrove M, Katz BG, Fahlquist LS, Crandall CA, Lindgren RJ (2014) Factors affecting public-supply well vulnerability in two Karst aquifers. Ground Water 52:63–75. doi:10.1111/gwat.12201

Nicollin F, Gibert D, Lesparre N, Nussbaum C (2010) Anisotropy of electrical conductivity of the excavation damaged zone in the Mont Terri Underground Rock Laboratory. Geophys J Int 181(1): 303–320. doi:10.1111/j.1365-246X.2010.04517.x

Nouioua I et al (2013) The application of GPR and electrical resistivity tomography as useful tools in detection of sinkholes in the Cheria Basin (northeast of Algeria). Environ Earth Sci 68(6):1661–1672. doi:10.1007/s12665-012-1859-9

NSW Department of Primary Industries (2012) Water sharing plan for the Macquarie Bogan unregulated and alluvial water sources: background document. http://www.water.nsw.gov.au. Accessed 15 Mar 2015

Osborne RAL (2001) Karst geology of wellington caves: a review. Helictite 37(1):3–12

Osborne RAL (2007) Cathedral cave, Wellington caves, New South Wales, Australia: a multiphase, non-fluvial cave. Earth Surf Process Landf 32(14):2075–2103. doi:10.1002/esp.1507

Osborne RAL (2010) Rethinking eastern Australian caves. Geol Soc Lond Spec Publ 346(1):289–308. doi:10.1144/sp346.15

Palmer A (1986) Prediction of contaminants paths in Karst aquifers. Proceedings of the conference Environmental Problems in Karst Terranes and their Solutions, Bowling Green, KY, 28–30 October 1986, pp 32–53

Pánek T et al (2010) Gravitationally induced caves and other discontinuities detected by 2D electrical resistivity tomography: case studies from the Polish Flysch Carpathians. Geomorphology 123(1–2): 165–180. doi:10.1016/j.geomorph.2010.07.008

Qarqori KH, Rouai M, Moreau F, et al (2012) Geoelectrical tomography investigating and modeling of fractures network around Bittit Spring (Middle Atlas, Morocco). Int J Geophys 2012, 489634, 13 pp. doi 10.1155/2012/489634

Redhaounia B, Ilondo BO, Gabtni H, Sami K, Bédir M (2016) Electrical Resistivity Tomography (ERT) applied to Karst carbonate aquifers: case study from Amdoun, northwestern Tunisia. Pure Appl Geophys 173(4):1289–1303. doi:10.1007/s00024-015-1173-z

Reynolds JM (1997) An introduction to applied and environmental geophysics. Wiley, Chichester, UK

Smakhtin VU (2001) Low flow hydrology: a review. J Hydrol 240(3–4): 147–186. doi:10.1016/S0022-1694(00)00340-1

Soupios P, Papadopoulos N, Papadopoulos I, et al (2007) Investigation of waste disposal areas using electrical methods: a case study from Chania, Crete, Greece. Environ Geol 51(7):1249–1261. doi:10.1007/s00254-006-0418-7

Spate A, Gough JS, Thurgate M (2001) Karstic groundwater ecosystems in the Murray-Darling and Otway groundwater basins. Helictite 37(1):22–22

Spiegel RJ, Sturdivant VR, Owen TE (1980) Modeling resistivity anomalies from localized voids under irregular terrain. Geophysics 45: 1164–1183. doi:10.1190/1.1441115

Strusz D (1965) A note on the stratigraphy of the Devonian Garra Beds of NSW. J Proc R Soc NSW 98:85–90

Šumanovac F, Weisser M (2001) Evaluation of resistivity and seismic methods for hydrogeological mapping in karst terrains. J Appl Geophys 47(1):13–28. doi:10.1016/S0926-9851(01)00044-1

Thurgatel ME, Gough JS, Spate A, Eberhard S (2001) Subterranean biodiversity in New South Wales: from rags to riches. Rec West Aust Mus Suppl 64:37–47

Ward SH (1990) Resistivity and induced polarization methods. Geotech Environ Geophys 1:147–189

Wilkinson PB, Chambers JE, Lelliott M, Wealthall GP, Ogilvy RD (2008) Extreme sensitivity of crosshole electrical resistivity tomography measurements to geometric errors. Geophys J Int 173(1):49–62. doi:10.1111/j.1365-246X.2008.03725.x

Winter TC (1995) Recent advances in understanding the interaction of groundwater and surface water. Rev Geophys 33(S2):985–994. doi:10.1029/95rg00115

Winter TC, Harvey JW, Franke OL, Alley WM (1998) Groundwater and surface water: a single resource. US Geol Surv Circ 1139

Zhou W, Beck B, Adams A (2002) Effective electrode array in mapping karst hazards in electrical resistivity tomography. Environ Geol 42(8):922–928. doi:10.1007/s00254-002-0594-z